Postprint of: Szymkiewicz A., Helmig R., Comparison of conductivity averaging methods for one-dimensional unsaturated flow in layered soils, Advances in Water Resources, Vol. 34, Iss. 8 (2011), pp. 1012-1025, DOI: 10.1016/j.advwatres.2011.05.011

Comparison of conductivity averaging methods for one-dimensional unsaturated flow in layered soils

A. Szymkiewicz[a,*], R. Helmig[b]

[a] *Faculty of Civil and Environmental Engineering, Gdańsk University of Technology, ul. Narutowicza 11/12, 80-233 Gdańsk, Poland*
[b] *Institute of Hydraulic Engineering, University of Stuttgart, Pfaffenwaldring 61, 70569 Stuttgart, Germany*

Abstract

One of important factors influencing the accuracy of the numerical solution of 1D unsaturated flow equation (Richards' equation) is the averaging method applied to compute hydraulic conductivity between two adjacent nodes of the computational grid. A number of averaging schemes have been proposed in the literature for homogeneous soil, including arithmetic, geometric, upstream and integrated means, as well as more sophisticated approaches, based on the local solution of steady state flow between the neighboring nodes (Darcian means). Another group of methods have been developed for the case when a material interface is present between the nodes. They range from simple arithmetic averaging to more complex schemes using the pressure- and flux-continuity conditions at the interface. In this paper we compare several averaging schemes for a number of steady and unsteady flow problems in layered soils. The first group of methods is applied in the framework of the vertex-centered approach to spatial discretization, where the nodes are placed at the material interfaces, while the second group is used with the cell-centered approach, where the material interfaces are located between computational nodes. The resulting numerical schemes are evaluated in terms of accuracy and computational time. *It is shown that the averaging schemes based on Darcian mean principle (Szymkiewicz, 2009) used in the framework of either vertex-centered or cell-centered approach compare favourably*

*Corresponding author
Email addresses: adams@pg.gda.pl (A. Szymkiewicz), rainer.helmig@iws.uni-stuttgart.de (R. Helmig)

May 18, 2011

to other methods for a range of test cases.

Keywords: Richards' equation, Layered soil, Internodal conductivity

1. Introduction

Water flow in partially saturated porous medium is commonly described with a nonlinear partial differential equation, known as the Richards' equation (RE). Its one-dimensional form is often used in hydrological and agricultural engineering to predict changes of water content and fluxes in the soil profile, which in turn can be used as input in larger scale hydrological models or contaminant transport models. The same equation can be also used to simulate moisture transport in building materials or other industrial porous materials. For the case of one-dimensional flow in an arbitrary spatial direction it can be written in the following form:

$$\frac{\partial \theta(h)}{\partial t} - \frac{\partial}{\partial z}\left[K(h)\left(\frac{\partial h}{\partial z} - \gamma\right)\right] = 0 \tag{1}$$

where t is time, z – spatial coordinate, h – water potential head (due to capillary and adsorption forces), θ – volumetric water content, $K(h)$ – hydraulic conductivity and γ represents the component of mass force acting in the direction of z, normalized with respect to the gravitational force. For horizontal flow $\gamma = 0$, for vertical flow with z oriented positively downwards $\gamma = 1$ and for flow in an inclined column $0 < \gamma < 1$ (values larger than one are also possible, for example for flow in a centrifuge). Eq. (1) can be extended by adding terms representing water and soil skeleton compressibility or source/sink terms, but such modifications do not affect the analysis presented in this paper. The unsaturated flow is characterized by highly nonlinear relations between h, θ and K, known as the hydraulic functions. The conductivity can be expressed as a product of the hydraulic conductivity at saturation K_s and the relative conductivity, depending on the water potential head $K_r(h)$. The hydraulic functions are often described by analytical formulas of Brooks and Corey [1] or van Genuchten–Mualem [3, 2], but many other models have been proposed. The nonlinearity of RE has important implications for its numerical solution, requiring appropriate time and space discretization schemes. Here we focus on the issues related to spatial discretization.

Spatial discretization of Eq. (1) is usually performed with low order finite difference method (FDM) or finite element method (FEM) [e.g. 4, 5, 6, 7, 8], although mixed-hybrid FEM [9] and discontinuous Galerkin FEM [10, 11] schemes were also proposed. Since in the FEM discretization mass-lumping must be applied to avoid oscillations [4], standard low-order FEM leads to essentially the same discrete equations as FDM. In each case it is necessary to estimate the average value of the hydraulic conductivity between adjacent nodes in order to compute the corresponding water flux. The most popular averaging schemes include arithmetic, geometric, upstream and integrated means. As shown by numerous studies [12, 13, 14, 15, 9, 16, 17, 18, 19] the accuracy of the numerical solution is sensitive to the choice of the averaging method, especially on coarser grids. The error can be significantly reduced by using adaptive grid refinement [e.g. 20, 21, 11] or by using a transformed variable instead of the water potential head in Eq. (1) [e.g. 22, 23], however such approaches imply additional algorithmic complexity. Thus, there is still some interest in developing improved averaging schemes that can be used in the framework of standard fixed-grid numerical algorithms.

Previous research showed that a significant improvement in accuracy can be obtained by using the so-called Darcian means approach, proposed by Warrick [24]. According to this method the average conductivity is chosen in such a manner that the resulting flux is equal to the flux obtained from the solution of steady state flow equation between the two nodes. Consequently, the internodal conductivity depends on the distance between the nodes, except for the case of horizontal flow. For most $K(h)$ functions the computation of "true" Darcian means require numerical solution of steady state problem, which makes this method unsuitable for practical application. It can be used, however, as a starting point for the development of approximate averaging formulas, which can be more readily implemented in practice. Such formulas were proposed by Baker [25], Baker et al. [16], Baker [26], Gastó et al. [18] and more recently by Szymkiewicz [19]. The latter one was shown to provide relatively accurate results for a wide range of conductivity functions and grid sizes.

An additional level of complexity is added when the porous material under consideration has layered structure. In such a case two basic approaches to spatial discretization can be distinguished. Adopting the framework of the finite volume method (FVM), we can call them vertex-centered (VC) and cell-centered (CC), respectively. In the first case, nodes are placed at the material interfaces and between them, so that the medium between neigh-

boring nodes is always homogeneous [e.g. 18, 7]. Consequently, the averaging schemes developed for homogeneous media can be applied. On the other hand the discontinuity in $\theta(h)$ function has to be taken into account when the storage term in Eq. (1) is evaluated at the interfacial node [27]. In the second approach the nodes are located at the centers of homogeneous grid cells [e.g. 28, 6, 23], which means that a unique $\theta(h)$ relation is associated with each node, but the material heterogeneity must be taken into account when computing the average conductivity between two neighboring cells which belong to different layers. Each discretization scheme can be used in conjunction with various conductivity averaging methods.

The objectives of this work are: first – to evaluate the accuracy of four selected averaging schemes used with the CC approach by comparing them to the Darcian means obtained from the steady state solution of RE for a two-layer medium, and second – to compare the performance of several VC and CC schemes for unsteady flow problems. To our knowledge no such analysis has been undertaken before, since previous papers focused on either vertex-centered or cell-centered schemes, but did not compare them directly to each other.

2. Spatial discretization and conductivity averaging schemes

2.1. Vertex-centered discretization

In both approaches to spatial discretization the solution domain is first divided into a number of cells, in such a way that each cell is homogeneous. In the VC approach (Fig. 1) the computational nodes are placed at the vertices (which in 1D are equivalent to cell edges), including the outer boundaries of the domain and then a dual mesh of control volumes is build in such a way that the boundaries of the control volumes are located midway between neighboring nodes. Consequently, control volumes built around material interfaces are heterogeneous and consist of two sub-volumes with different material properties. On the other hand, the medium between each pair of neighboring nodes is homogeneous. The resulting semi-discrete form

of Eq. (1) is as follows:

$$L_i^{(1)}\frac{\mathrm{d}\theta^{(1)}(h_i)}{\mathrm{d}t} + L_i^{(2)}\frac{\mathrm{d}\theta^{(2)}(h_i)}{\mathrm{d}t} - K^{(2)}_{i+\frac{1}{2}}(h_i, h_{i+1}) \cdot \left[\frac{h_{i+1}-h_i}{\Delta z_{i+\frac{1}{2}}} - \gamma\right] + K^{(1)}_{i-\frac{1}{2}}(h_{i-1}, h_i) \cdot \left[\frac{h_i - h_{i-1}}{\Delta z_{i-\frac{1}{2}}} - \gamma\right] = 0 \quad (2)$$

where $L_i^{(1)}$ and $L_i^{(2)}$ denote the lengths of the parts of grid cell i occupied by porous materials (1) and (2) respectively, $\Delta z_{i+\frac{1}{2}}$ is the distance between node i and $i+1$ and $\Delta z_{i-\frac{1}{2}}$ – the distance between node $i-1$ and i (see Fig. 1).

The average conductivity between each pair of nodes, say between i and $i+1$, can be computed using one of the methods developed for homogeneous media:

- arithmetic mean (VC-ARIT)

$$K^{(2)}_{i+\frac{1}{2}} = \frac{1}{2}\left(K^{(2)}(h_i) + K^{(2)}(h_{i+1})\right) \quad (3)$$

- geometric mean (VC-GEOM)

$$K^{(2)}_{i+\frac{1}{2}} = \sqrt{K^{(2)}(h_i) \cdot K^{(2)}(h_{i+1})} \quad (4)$$

- upstream mean (VC-UPS)

$$K^{(2)}_{i+\frac{1}{2}} = \begin{cases} K^{(2)}(h_i) & \text{if} \quad \frac{\Delta h_{i+\frac{1}{2}}}{\Delta z_{i+\frac{1}{2}}} - \gamma \leq 0 \\ K^{(2)}(h_{i+1}) & \text{if} \quad \frac{\Delta h_{i+\frac{1}{2}}}{\Delta z_{i+\frac{1}{2}}} - \gamma > 0 \end{cases} \quad (5)$$

where $\Delta h_{i+\frac{1}{2}}$ denotes the difference of the water potential head between node $i+1$ and i, $\Delta h_{i+\frac{1}{2}} = h_{i+1} - h_i$,

- integrated mean

$$K^{(2)}_{i+\frac{1}{2}} = K^{(2)}_{INT}(h_i, h_{i+1}) = \\ = \frac{1}{\Delta h_{i+\frac{1}{2}}} \int_{h_i}^{h_{i+1}} K^{(2)}(h)\mathrm{d}h = \frac{\Phi^{(2)}(h_{i+1}) - \Phi^{(2)}(h_i)}{\Delta h_{i+\frac{1}{2}}} \quad (6)$$

  where $\Phi^{(2)}$ denotes the flux potential function (also known as Kirchhoff transformed variable) for material (2), $\Phi^{(2)}(h_i) = \int_{-\infty}^{h_i} K^{(2)}(\psi)\mathrm{d}\psi$.

Numerical experiments published in the literature show that none of the methods listed above is really universal, because their performance depends on the shape of the conductivity function, initial-boundary conditions of the problem under consideration and grid size Δz [12, 13, 14, 15, 16, 18, 9, 19]. A more accurate averaging technique is based on the assumption that the average conductivity should reproduce the steady-state flow rate between the two considered nodes, with the water potential values h_i and h_{i+1} taken as the boundary conditions. This approach, introduced by Warrick [24] is called Darcian mean, because it implies the equivalence between the discrete and differential (continuous) forms of the Darcy's law:

$$q_{st} = -K^{(2)}_{i+\frac{1}{2}} \left(\frac{\Delta h_{i+\frac{1}{2}}}{\Delta z_{i+\frac{1}{2}}} - \gamma \right) = -K^{(2)}(h) \left(\frac{\mathrm{d}h}{\mathrm{d}z} - \gamma \right) \quad (7)$$

where q_{st} is the uniform steady flux between nodes. The differential form of Darcy's law can be integrated as follows:

$$\int_{z_i}^{z_{i+1}} \mathrm{d}z = -\int_{h_i}^{h_{i+1}} \frac{K^{(2)}(h)\mathrm{d}h}{q_{st} - \gamma K^{(2)}(h)} \quad (8)$$

For horizontal flow with $\gamma = 0$ one obtains:

$$\Delta z_{i+\frac{1}{2}} = -\frac{1}{q_{st}} \int_{h_i}^{h_{i+1}} K^{(2)}(h)\mathrm{d}h \quad (9)$$

Comparing this result with the discrete form of Darcy's law appearing in Eq. (7) gives:

$$K^{(2)}_{i+\frac{1}{2}} = \frac{1}{\Delta h_{i+\frac{1}{2}}} \int_{h_i}^{h_{i+1}} K^{(2)}(h)\mathrm{d}h = K^{(2)}_{INT}(h_i, h_{i+1})$$

Thus, the integrated mean corresponds to the Darcian mean for horizontal flow. In a general case of $\gamma > 0$ the Darcian mean is different from any of the simple averages listed above.

For exponential conductivity function integration of the steady flow equation can be carried out analytically, leading to an exact formula [25], but in the case of more complicated $K(h)$ functions the integration must be done numerically, which requires exceedingly large effort when solving unsteady flow problems. However, the concept of Darcian mean can be used to develop approximate averaging schemes which are more accurate than the standard formulas, and on the other hand relatively easy to implement. For example Baker [26] proposed an approximation for arbitrary conductivity function based on the exact result for the exponential function [25]. Since this method requires inverting the conductivity function to obtain $h(K)$ it cannot be readily applied to the standard van Genuchten–Mualem model. Gastó et al. [18] suggested a weighted arithmetic average of the nodal conductivities, where the weighting coefficient is calculated from an analytical formula depending on the nodal conductivities, internodal distance and parameters of the conductivity function according to Brooks–Corey or van Genuchten–Mualem models. The application of this approach is limited to those two conductivity models and to Δz smaller than the parameter which scales the water potential head in the respective function (i.e. the air-entry pressure for BC and $1/\alpha$ for VGM).

In this paper we focus on the approximation proposed by Szymkiewicz [19], which can be applied to an arbitrary conductivity function. It consists of three formulas, the choice depending on the relation between the gradient of capillary and gravity potential:

- if $\frac{\Delta h_{i+\frac{1}{2}}}{\Delta z_{i+\frac{1}{2}}} < 0$ both capillary and gravity gradients are directed downward (infiltration in dry soil):

$$K^{(2)}_{i+\frac{1}{2}} = \max\left(K^{(2)}_{INT}(h_i, h_{i+1}), \frac{\gamma \cdot K^{(2)}(h_i)}{\gamma - \Delta h_{i+\frac{1}{2}}/\Delta z_{i+\frac{1}{2}}}\right) \tag{10}$$

- if $\gamma > \frac{\Delta h_{i+\frac{1}{2}}}{\Delta z_{i+\frac{1}{2}}} > 0$ the flow is in downward direction, but the capillary gradient acts oppositely to the gravity (drainage or infiltration towards

water table):

$$K^{(2)}_{i+1/2} = \min\left(K^{(2)}(h_a), \frac{\gamma \cdot K^{(2)}(h_i)}{\gamma - \Delta h_{i+\frac{1}{2}}/\Delta z_{i+\frac{1}{2}}}\right) \tag{11}$$

where $h_a = h_{i+1} - \dfrac{(\Delta h_{i+\frac{1}{2}})^2}{\gamma \Delta z_{i+\frac{1}{2}}}$;

- if $\frac{\Delta h_{i+\frac{1}{2}}}{\Delta z_{i+\frac{1}{2}}} > 1$ the flow is in upward direction (evaporation or capillary rise):

$$K^{(2)}_{i+\frac{1}{2}} = \frac{\Delta z_{i+\frac{1}{2}} \cdot K_a \cdot K_b}{(\Delta z_{i+\frac{1}{2}} - \delta z) \cdot K_a + \delta z \cdot K_b} \tag{12}$$

where $K_a = K^{(2)}_{INT}(h_i, h_b)$, $K_b = K^{(2)}(h_b)$, $h_b = h_{i+1} - \Delta z_{i+\frac{1}{2}}$ and

$$\delta z = \frac{-\Delta h_{i+\frac{1}{2}} + \sqrt{(\Delta h_{i+\frac{1}{2}})^2 + 4(K_b/K_a - 1)\gamma(\Delta h_{i+1/2} - \gamma \Delta z_{i+1/2})\Delta z_{i+\frac{1}{2}}}}{2\gamma(K_b/K_a - 1)}$$

The above approximations ensure that when $\frac{\Delta h_{i+\frac{1}{2}}}{\Delta z_{i+\frac{1}{2}}}$ approaches 0 or γ from either side, the average conductivity $K^{(2)}_{i+\frac{1}{2}}$ tends to the value at the upper node $K^{(2)}(h_i)$, which is consistent with the Darcian averaging principles [16, 26]. The combination of this averaging technique with VC discretization will be referred to as VC-SZYM.

2.2. Cell-centered discretization

An alternative approach to spatial discretization is to use homogeneous cells of the primal grid as the control volumes (Fig. 2), and to place nodes at their centers. In this case, a unique capillary function is associated with each node, but whenever the boundary between control volumes coincides with a material interface, a discontinuity of the conductivity function should be taken into account when averaging is applied. For example, the following

semi-discrete equation results for the control volume around node i:

$$L_i \frac{\mathrm{d}\theta^{(1)}(h_i)}{\mathrm{d}t} - K^{(1,2)}_{i+\frac{1}{2}}(h_i, h_{i+1}) \cdot \left[\frac{h_{i+1} - h_i}{\Delta z_{i+\frac{1}{2}}} - \gamma \right] + K^{(1)}_{i-\frac{1}{2}}(h_{i-1}, h_i) \cdot \left[\frac{h_i - h_{i-1}}{\Delta z_{i-\frac{1}{2}}} - \gamma \right] = 0 \quad (13)$$

In the above equation $K^{(1)}$ denotes the average conductivity value in the homogeneous layer of material (1), computed with one of the schemes listed above, while $K^{(1,2)}$ is the average value in the heterogeneous layer. One straightforward option to approximate $K^{(1,2)}$ is to use the arithmetic mean of the nodal conductivities, by analogy to the homogeneous case:

$$K^{(1,2)}_{i+\frac{1}{2}} = \frac{1}{2}\left(K^{(1)}_s \cdot K^{(1)}_r(h_i) + K^{(2)}_s \cdot K^{(2)}_r(h_{i+1})\right) \quad (14)$$

This approach is used for example in the well known HYDRUS-1D numerical code [8], and will be referred to as CC-ARIT.

Another possible method is to use the harmonic averaging of the saturated conductivities and upstream-weighted relative conductivity:

$$K^{(1,2)}_{i+\frac{1}{2}} = K^{(1,2)}_{s,i+\frac{1}{2}} \cdot K^{(1,2)}_{r,i+\frac{1}{2}} \quad (15)$$

$$K^{(1,2)}_{s,i+\frac{1}{2}} = \left[\Delta z^{(1)}_{i+\frac{1}{2}} + \Delta z^{(2)}_{i+\frac{1}{2}}\right] \cdot \left(\frac{\Delta z^{(1)}_{i+\frac{1}{2}}}{K^{(1)}_s} + \frac{\Delta z^{(2)}_{i+\frac{1}{2}}}{K^{(2)}_s} \right)^{-1} \quad (16)$$

$$K^{(1,2)}_{r,i+\frac{1}{2}} = \begin{cases} K^{(1)}_r(h_i) & \text{if } \frac{\Delta h_{i+\frac{1}{2}}}{\Delta z_{i+\frac{1}{2}}} - \gamma \leq 0 \\ K^{(2)}_r(h_{i+1}) & \text{if } \frac{\Delta h_{i+\frac{1}{2}}}{\Delta z_{i+\frac{1}{2}}} - \gamma > 0 \end{cases} \quad (17)$$

where $\Delta z^{(1)}_{i+\frac{1}{2}}$ and $\Delta z^{(2)}_{i+\frac{1}{2}}$ refer to the parts of the internodal distance at each side of the material interface (Fig. 2). This scheme will be referred to as CC-UPS. It gives the correct value of $K^{(1,2)}_{i+\frac{1}{2}}$ for saturated flow. On the other hand the use of upstream mean of relative conductivity prevents the rise of unphysical oscillations in the solution of advection dominated flow [29, 30].

Yet another approach was proposed by Romano et al. [28]. It makes use of the physically based assumption that the water potential head and flux

should be continuous across the interface. Romano et al. [28] proposed to introduce two "ghost nodes" (Fig. 3). One of them is located above the interface and extrapolates the pressure profile from the lower layer, while the other one is located below the interface and extrapolates the pressure profile from the upper layer. Assuming that the interface is located mid-way between the nodes, Romano et al. [28] proposed to write the potential head and flux continuity conditions in the following form:

$$\frac{1}{2} \cdot (h_i + \bar{h}_{i+1}) = \frac{1}{2} \cdot (\bar{h}_i + h_{i+1}) \tag{18}$$

$$-K^{(1)}_{i+\frac{1}{2}}(h_i, \bar{h}_{i+1}) \cdot \left[\frac{\bar{h}_{i+1} - h_i}{\Delta z_{i+\frac{1}{2}}} - \gamma \right] = -K^{(2)}_{i+\frac{1}{2}}(\bar{h}_i, h_{i+1}) \cdot \left[\frac{h_{i+1} - \bar{h}_i}{\Delta z_{i+\frac{1}{2}}} - \gamma \right] \tag{19}$$

where $\bar{h}_i$ and $\bar{h}_{i+1}$ denote the potential head values at the ghost nodes, and the average conductivity for each of the materials is equal to the geometric mean of the nodal values:

$$K^{(1)}_{i+\frac{1}{2}}(h_i, \bar{h}_{i+1}) = \sqrt{K^{(1)}(h_i) \cdot K^{(1)}(\bar{h}_{i+1})}$$

$$K^{(2)}_{i+\frac{1}{2}}(\bar{h}_i, h_{i+1}) = \sqrt{K^{(2)}(\bar{h}_i) \cdot K^{(2)}(h_{i+1})}$$

The nonlinear system of equations (18)–(19) have to be solved iteratively for each material interface. The internodal conductivity is then computed as the harmonic average of the conductivities in the two sub-layers:

$$K^{(1,2)}_{i+\frac{1}{2}} = \frac{2 \cdot K^{(1)}_{i+\frac{1}{2}}(h_i, \bar{h}_{i+1}) \cdot K^{(2)}_{i+\frac{1}{2}}(\bar{h}_i, h_{i+1})}{K^{(1)}_{i+\frac{1}{2}}(h_i, \bar{h}_{i+1}) + K^{(2)}_{i+\frac{1}{2}}(\bar{h}_i, h_{i+1})} \tag{20}$$

This approach will be referred to as CC-ROM. While it was shown to be more accurate than standard arithmetic and geometric weighting in the test cases considered by Romano et al. [28] and Brunone et al. [6], it raises two questions. First, it is not clear, why the authors decided to introduce the ghost values of the potential, which do not have any physical interpretation, instead of using the interface potential directly (see below). Second, geometric averaging of conductivities in some cases leads to significant errors, for example when simulating infiltration in dry sand [e.g. 18, 19].

Finally we can consider a more general approach, based on the flux continuity condition given by Eq. (19), where the average conductivities in the sub-layers are computed using the interfacial value of the potential head h_c, instead of "ghost" nodes (Fig. 3):

$$-K^{(1)}_{i+\frac{1}{2}}(h_i, h_c) \cdot \left[\frac{h_c - h_i}{\Delta z^{(1)}_{i+\frac{1}{2}}} - \gamma \right] = -K^{(2)}_{i+\frac{1}{2}}(h_c, h_{i+1}) \cdot \left[\frac{h_{i+1} - h_c}{\Delta z^{(2)}_{i+\frac{1}{2}}} - \gamma \right] \quad (21)$$

The average conductivities between the node i and interface, $K^{(1)}_{i+\frac{1}{2}}(h_i, h_c)$, and between the interface and node $i+1$, $K^{(2)}_{i+\frac{1}{2}}(h_c, h_{i+1})$, can be approximated with any scheme suitable for homogeneous medium. The nodes can be positioned asymmetrically with respect to the interface. The resulting nonlinear equation has to be solved iteratively for each interface, similarly to the method of Romano et al. [28]. Once the value of the interfacial potential head h_c and the corresponding values of $K^{(1)}_{i+\frac{1}{2}}(h_i, h_c)$ and $K^{(2)}_{i+\frac{1}{2}}(h_c, h_{i+1})$ are obtained, the average conductivity between the nodes i and $i+1$ can be calculated as the weighted harmonic mean:

$$K^{(1,2)}_{i+\frac{1}{2}} = \left[\Delta z^{(1)}_{i+\frac{1}{2}} + \Delta z^{(2)}_{i+\frac{1}{2}} \right] \cdot \left[\frac{\Delta z^{(1)}_{i+\frac{1}{2}}}{K^{(1)}_{i+\frac{1}{2}}(h_i, h_c)} + \frac{\Delta z^{(2)}_{i+\frac{1}{2}}}{K^{(2)}_{i+\frac{1}{2}}(h_c, h_{i+1})} \right]^{-1} \quad (22)$$

In this work we apply this approach in conjunction with the Darcian averaging method proposed by Szymkiewicz [19], and denote it as CC-SZYM.

3. Evaluation of cell-centered conductivity averaging schemes for steady flow

The conductivity averaging schemes for homogeneous medium used in the framework of VC discretization were compared with exact Darcian means in a number of previous papers [16, 26, 19]. Here we focus on the case of heterogenous medium consisting of two layers, which arises in CC discretization scheme. To this end, we first computed the fluxes between two nodes placed symmetrically at both sides of the material interface using the CC-ARIT, CC-UPS, CC-ROM and CC-SZYM schemes. Those values were then compared to the flux obtained from the steady-state solution of RE for the domain between the two nodes. The steady state solution was obtained with

VC-ARIT scheme, but in order to make sure that it is not affected by the spatial discretization error the grid was refined iteratively, until the relative difference between the fluxes at two subsequent refinement levels was smaller than 0.1%. Two sets of simulations were performed – one using the Brooks–Corey–Burdine hydraulic functions:

$$\theta(h) = \begin{cases} \theta_r + (\theta_s - \theta_r) \cdot (h/h_e)^{-\lambda} & \text{if } h < h_e \\ 1 & \text{if } h \geq h_e \end{cases} \tag{23}$$

$$K(h) = \begin{cases} K_s \, (h/h_e)^{-2-3\lambda} & \text{if } h < h_e \\ K_s & \text{if } h \geq h_e \end{cases} \tag{24}$$

and the other one using van Genuchten–Mualem functions:

$$\theta(h) = \theta_r + (\theta_s - \theta_r) \cdot [1 + (h/h_g)^n]^{-m} \tag{25}$$

$$K(h) = \frac{K_s}{[1 + (h/h_g)^n]^{m/2}} \left[1 - \frac{(h/h_g)^{n-1}}{(1 + (h/h_g)^n)^m} \right]^2 \tag{26}$$

In the above equations θ_r is the residual water content, θ_s is the water content at saturation, h_e is the air-entry pressure head in the Brooks–Corey model, h_g is the pressure scaling parameter in the van Genuchten model, λ and n are parameters depending on the pore size distribution and $m = 1 - 1/n$. The soils characterized by these functions are referred to as BC-sand, BC-clay, VG-sand and VG-clay, respectively. Their parameters are listed in Table 1. They were taken from the database implemented in HYDRUS-1D software [8]. For each set of hydraulic functions a large number of simulations was performed, with varying sequence of the layers (sand over clay, clay over sand), distance between nodes, $\Delta z = \{1, 2, 5, 10, 20, 50, 100, 200, 500\}$ cm, and potential head values at the nodes, $h = \{10, 0, -1, -10, -100, -1000\}$ cm (for Brooks–Corey model the potential values were modified by adding negative value corresponding to h_b, as listed in Table 1 for respective soils).

For a given combination of parameters the error of any averaging scheme was defined as follows:

$$E_K = \log_{10} \frac{K}{K_{ref}} \tag{27}$$

where K was computed with the considered averaging scheme and K_{ref} was obtained from the steady state solution. In order to compare a large number of results, some representative error measures were introduced for each method of approximation:

- root-mean square error, $RMS(E_K)$
- maximum error value (largest overestimation), $\max(E_K)$
- minimum error value (largest underestimation), $\min(E_K)$

The values of these parameters are listed in Table 2 for soils characterized by Brooks-Corey functions and in Table 3 for the van Genuchten–Mualem functions. Moreover, for the schemes CC-ROM and CC-SZYM the values of the potential head at the interface can be compared with the values obtained from the fine-grid steady state simulation. The corresponding root mean square errors, denoted as $RMS(E_{hc})$ are also reported.

It can be seen that the averaging scheme CC-SZYM, based on approximation of the Darcian means, is much more accurate in predicting the value of steady-state average conductivity than the other three methods. CC-ROM is second best, but still can lead to over- or underestimation of the conductivity by several orders of magnitude. It can be also noted, that all methods are less accurate for van Genuchten–Mualem model than for Brooks–Corey model.

4. Unsteady flow examples

4.1. Introduction

The discretization in time of Eqs. (2) and (13) was carried out with the first order fully implicit scheme. At each time step the resulting set of nonlinear algebraic equations was solved using Newton method with line search. As the convergence criterion we assumed that at the current time step j the residual of Eq. (2) or (13) at any node i should not exceed $(10^{-12} + 10^{-6} \cdot \theta_i^j)$. This criterion ensured excellent mass balance for all simulations, with relative errors below $10^{-3}\%$. Adaptive time stepping algorithm was used, based on the number of Newton iterations required to achieve convergence. If more than 7 iterations were required, the next time step was reduced by 0.8, while for the number of iterations smaller than 3 it was multiplied by 1.25. This approach was consistently used in all simulations, in order to obtain comparable simulation times.

The five test cases presented below were chosen in such a way that they represent all flow types covered by the approach of Szymkiewicz [19], i.e. infiltration in dry soil, infiltration towards water table and capillary uptake. The examples also differ in the number of layers (from 2 to 5), and in the model

used for conductivity function *(Gardner, Brooks–Corey and van Genuchten-Mualem).*

For each case we performed simulations using five grid sizes. The finest one was either 0.5 cm or 1 cm, which is sometimes suggested as sufficiently fine to obtain accurate results when arithmetic averaging of conductivity is used [5]. The coarsest grid always corresponded to the minimum possible number of grid cells, i.e. one cell per soil layer. The reference solutions were obtained on very fine grid with $\Delta z = 1$ mm, and their reliability was checked by comparing several runs with different averaging schemes. *For each test case we provide tables with information about the runs for three selected discretizations, including errors, computational times (wall-clock time), and number of time steps (note that the errors are defined differently from case to case, depending on the formulation of the problem). Moreover, we show plots of error versus computational time based on the results for all five grid sizes.*

In *Test Cases C, D and E* the hydraulic functions (including the flux potential function Φ) were interpolated from a look-up table generated at the preprocessing stage. This allowed for fast computation of the integrals of van Genuchten–Mualem conductivity function required in formulas (10) and (12). Linear interpolation was used and in each case the table consisted of 100 irregularly spaced potential head values. The reference solutions in each case were obtained using direct evaluation of the hydraulic functions. In the first *and second* example, where Gardner and Brooks–Corey functions are used, the integrals can be easily evaluated analytically.

We evaluated performance of eight schemes applicable to any type of soil. These are VC-ARIT, VC-GEOM, VC-UPS, VC-SZYM, CC-ARIT, CC-ROM, CC-UPS and CC-SZYM. Moreover, we included the combination of VC discretization with the Darcian averaging scheme of Baker [25] (Test Cases A and B, VC-BAKER) and that of Gastó et al. [18] (Test Cases B,C,D and E, VC-GASTO).

4.2. Test case A

The first example is adapted from Brunone et al. [6] and represents infiltration towards water table. The solution domain consists of two equal layers (Fig. 4a). Each of them is characterized by Gardner hydraulic functions of

the following form:

$$\theta(h) = \theta_r + (\theta_s - \theta_r) \cdot \exp(-\frac{h}{h_g}) \tag{28}$$

$$K(h) = K_s \cdot \exp(-\frac{h}{h_g}) \tag{29}$$

Parameters of the hydraulic functions are listed in Table 1. Note that the materials differ only in the value of the conductivity at saturation K_s. Brunone et al. [6] assumed as the initial condition the water potential profile corresponding to a steady downward flux of 0.001 cm/h, and then ran the simulation with boundary flux increased to 0.9 cm/h. In our example we started with hydrostatic pressure distribution as the initial condition, ran the simulation for 120 h with the boundary flux equal to 0.001 cm/h to reach steady state, and then instantaneously increased the flux to the value 0.9 cm/h, and ran the simulation for another 10 h . The time step varied in the range 10^{-6} to 0.1 h. The reference solution profile for the final time shown in Fig. 6a closely corresponds to the profile for $t = 10$ h shown by Brunone et al. [6]. The simulations were carried out for $\Delta z = 1$, 4, 20, 50, and 100 cm.

As the error measures we used the root mean square error of the water potential head values at computational nodes and the root mean square error of the water content values. In each case values from two time levels were included: $t = 120$ h and $t = 130$ h.

$$ERR_h = \sqrt{\frac{1}{2M}\left[\sum_{i=1}^{M}\left(h_i^{t=120h} - h_{i,ref}^{t=120h}\right)^2 + \sum_{i=1}^{M}\left(h_i^{t=130h} - h_{i,ref}^{t=130h}\right)^2\right]}$$

$$ERR_\theta = \sqrt{\frac{1}{2M}\left[\sum_{i=1}^{M}\left(\theta_i^{t=120h} - \theta_{i,ref}^{t=120h}\right)^2 + \sum_{i=1}^{M}\left(\theta_i^{t=130h} - \theta_{i,ref}^{t=130h}\right)^2\right]}$$

where M is the number of nodes in the computational grid, and the subscript ref denotes the values from the reference solution. In the case of VC schemes the volumetric water content at the interface node was computed as the arithmetic average of the values for the two materials. The values of ERR_h and ERR_θ for three selected grid sizes are listed in Table 4 along with the number of time steps and and time required to complete each simulation.

It can be seen that the relative accuracy of various schemes is different with respect to the water potential and water content, due to the nonlinear

relations between those two parameters. For the finest discretization, the best results are obtained with VC-BAKER, while CC-ROM, VC-GEOM and VC-ARIT are also very accurate. This is in agreement with the results reported by Brunone et al. [6] for a relatively fine grid of 0.25 cm, where their scheme was superior to the CC-ARIT approach, as used by HYDRUS-1D. However, at the coarsest discretization level CC-ROM, VC-GEOM and VC-ARIT are relatively inaccurate with respect to the water potential, although CC-ROM retains high accuracy in terms of water content. In contrast, the VC schemes based on Darcian means, i.e. VC-SZYM and VC-BAKER are the most accurate with respect to the water potential, but relatively inaccurate in terms of water content. In Fig. 5 the relation between ERR_θ and computational time can be seen. For coarse discretizations the most efficient method is CC-ARIT, but it converges slowly. On the other hand for finer discretizations VC-ARIT seems to outperform all other methods, since it is fast and accurate. It should be noted, however, that this example is not very challenging with respect to the numerical solution, due to relatively smooth hydraulic functions. Water content profiles obtained with various averaging schemes for $\Delta z = 20$ cm (Fig. 6) show good qualitative agreement with the reference solution (profile obtained with VC-BAKER, not shown here, is virtually indistinguishable from the profile given by VC-SZYM).

4.3. Test Case B

In this example we used the same geometry and spatial discretizations as in Test Case A, but the two soil layers were characterized by Brooks–Corey functions (upper layer – BC-sand, lower layer – BC-clay, parameters listed in Table 1). The initial and boundary conditions ((Fig. 4b) were chosen in such a way that a saturated zone develops near the interface. Parameters of the numerical simulations are listed in Table 5. This example was more challenging and the schemes based on geometric averaging performed poorly in some cases. VC-GEOM did not converge for the two coarsest discretizations, while CC-ROM required a large number of iterations to converge for $\Delta z = 20$ and 50 cm. Due to strong nonlinearity of the hydraulic functions the errors in water potential show non-monotonic behavior, unrelated to the errors in water content (the results for grid sizes $\Delta z = 4$ and 50 cm, not shown in Table 5 support this conclusion also for VC-SZYM and VC-BAKER). The errors in water content decrease monotonically for most schemes except VC-GEOM, CC-ROM and VC-SZYM at coarser grids (Fig. 7). From the latter figure it can be seen that the schemes VC-SZYM and VC-BAKER outper-

form other methods except for the coarsest grids where CC-UPS is slightly better. Good results are also obtained with VC-GASTO, but this scheme can be used only for the two finest levels of discretization. The final profiles of the water content for $\Delta z = 20$ cm are plotted in Fig. 8. It can be seen that both VC-SZYM and CC-SZYM closely follow the reference profile (the same is true for VC-BAKER, not shown here, which closely coincides with VC-SZYM). The methods based on arithmetic and upstream averaging show qualitative agreement with the reference solution, but predict more diffused wetting fronts. The profiles obtained with VC-GEOM and CC-ROM differ significantly from the reference, showing large saturated zone in the upper part of the sand layer. This is caused by the underestimation of the hydraulic conductivity when geometric averaging is used for infiltration in dry soil.

4.4. Test Case C

This example is taken from the paper by Hills et al. [27] and was examined previously by Gastó et al. [18]. It concerns infiltration in dry soil profile (Fig. 4c), consisting of alternating layers of Berino loamy fine sand and Glendale clay loam, both characterized by van Genuchten –Mualem hydraulic functions (see Table 1 for the actual values of the parameters). The initial pressure distribution is uniform and corresponds to relatively dry conditions. At the top a constant water head is imposed, while at the bottom the free drainage condition is applied. The simulation time is 48 h, the time step varied in the range 10^{-6} to 0.1 h. Following Gastó et al. [18] we used the relative error in the amount of water that infiltrated in the domain as the error measure:

$$REL_{INF} = \frac{W - W_{ref}}{W_{ref}} 100\%$$

where $W_{ref} = \int(\theta_{ref} - \theta_{init})dz$ is the cumulative infiltration predicted by the reference solution, equal to 14.11 cm, $W = \int(\theta - \theta_{init})dz$ is the amount of infiltrated water predicted by the considered model and θ_{init} is the water content corresponding to the initial water potential distribution. Simulations were performed for grid sizes of 0.5, 1, 5, 10, and 20 cm. The details of simulations for three selected discretizations can be seen in Table 6.

The plots of error versus computational time are shown in Fig. 9. The irregular convergence pattern for some methods can be partially explained by the fact that the reference solution was obtained using direct evaluation of hydraulic functions while in other simulations linear interpolation from pre-processed table was used. Thus, even for very fine discretisation an error

of the order of a few percent can be expected due to linear interpolation. Nevertheless, it can be seen that the methods based on Darcian averaging (VC-GASTO, VC-SZYM and CC-SZYM) outperform other methods on coarser grids. On finer grids, comparable or better results can be achieved with VC-GEOM and CC-ROM, but these two schemes become very inaccurate as the spatial step increases. The water content profiles in Fig. 10 show that schemes based on geometric averaging produce unreliable results for $\Delta z = 10$*, due to underestimation of the infiltration rate. For coarser discretizations the errors are even larger, however it should be noted that CC-ROM was more accurate than VC-GEOM.*

4.5. Test Case D

The next example concerns upward flow in a two-layer medium (Fig. 4d). The initial condition is hydrostatic potential distribution. At the bottom constant potential head $h = 0$ is maintained, while at the surface the potential head is lowered to -1000 cm. The simulation was run for $t = 240$ h and the time step varied in the range 10^{-6} to 0.5 h. According to the reference solution, the cumulative amount of evaporated water was $Q_{top,ref} = 0.38$ cm. The relative error in the amount of evaporated water was defined as:

$$REL_{EV} = \frac{Q_{top} - Q_{top,ref}}{Q_{top,ref}} 100\%$$

In contrast to the previous case, here the integral of the water content at the final time is not a convenient measure, because of the possible influence of water inflow from the lower boundary. Simulations were performed for grid sizes of 0.5, 1, 5, 25, and 50 cm. The parameters of selected simulations are listed in Table 7 and the plots of error versus time are shown in Fig. 11.

Similarly to the previous example, the plots show non-monotonic convergence for VC-SZYM and CC-SZYM schemes, due to the influence of errors related to the interpolation of hydraulic functions. Schemes based on arithmetic and upstream averaging show good convergence, but the errors for coarse discretizations are unacceptably large, with the cumulative evaporation overpredicted by several orders of magnitude. This can be explained by the fact that both approaches produce average conductivity of the same order of magnitude as the conductivity of the more wet node. Thus, the limiting influence of the dry layer at the soil surface is neglected. On the other hand, the schemes based on geometric averaging (VC-GEOM and CC-ROM) largely underestimate the amount of evaporated water, regardless of the grid size.

Apparently, when the internodal conductivity is computed as the geometric mean too much weight is assigned to the conductivity of the weakly permeable node at the soil surface. Note also that, in contrast to Test Cases B and C, here VC-GASTO has no advantage over simple averaging methods.

Additional insights can be obtained from the analysis of the final profiles of water potential head as shown in Fig. 11. It can be seen that the profiles produced by VC-SZYM and CC-SZYM are very close to the reference one. The methods based on geometric averaging tend to underestimate the internodal conductivity when one of the nodes is very dry, as it is the case in the uppermost part of the profile. As the system tends to steady state low conductivity must be compensated for by a larger gradient of the water potential head. Conversely, when arithmetic or upstream averaging is used, the conductivity near surface is overpredicted, because more weight is associated with the conductivity of the lower (more wet) node. Smaller differences between conductivities in the upper and lower parts of the domain lead to smaller differences in water potential gradients when steady state is approached.

4.6. Test Case E

The final example also concerns upward flow with similar initial and boundary conditions, but this time three soil layers are present (Fig. 4e). A very long process was considered, with the final time $t = 50000$ h and the time step varying in the range 10^{-6} to 1000 h. Simulations were performed for grid sizes of 0.5, 1, 4, 10, and 40 cm. The parameters of selected simulations are listed in Table 8, while Fig. 13 shows the plots of error versus time.

The performance of various averaging schemes is generally similar to the previous example, except for CC-UPS which has better accuracy, comparable to VC-SZYM and CC-SZYM. Again, arithmetic averaging tends to overestimate the amount of evaporation, while geometric averaging results in an underestimation. The profiles of water potential head $\Delta z = 10$ cm are shown in Fig. 14. In dry conditions the permeability of sand is much smaller than that of clay, and consequently the water potential gradient in the central sand layer is larger than the gradients in the upper and lower clay layers. Similarly to the previous case, VC-GEOM and CC-ROM produced gradients in the sand layer larger than the reference solution, while VC-UPS, VC-ARIT and CC-ARIT overestimated the conductivity of sand and underestimated the potential gradients. Both VC-SZYM and CC-SZYM show remarkable agreement with the fine scale solution. At finer grids these two schemes required more

time steps and consequently longer computational times than other methods, but this was compensated for by significantly better accuracy. Thus, they have advantage in efficiency over other methods for the whole range of discretization. It should be noted that comparable efficiency is achieved with CC-UPS. On the other hand, VC-GASTO is relatively inaccurate and requires considerable computational time.

5. Discussion and conclusions

Numerical results presented above show that the conductivity averaging schemes based on approximation of Szymkiewicz [19] perform generally better than the other considered methods. This does not mean that VC-SZYM and CC-SZYM outperform all other methods in all test cases. For example in Test Case A their performance was average related to other schemes. However in other examples, which were more challenging numerically, they consistently provided solutions close to the reference for the whole range of discretizations. In contrast, schemes based on simple averaging approaches (arithmetic, geometric or upstream) often produced excessively large errors in cumulative fluxes or unrealistic water content profiles. VC-SZYM and CC-SZYM also compare favorably to other schemes based on Darcian averaging principle, i.e. VC-BAKER and VC-GASTO. The former one performed similarly or slightly better than VC-SZYM, but cannot be easily applied to van Genuchten–Mualem conductivity functions. The latter one is not applicable for coarser grids and was shown to be significantly less accurate in Test Cases D and E, dealing with evaporation.

It can be shown that the Darcian mean, which represents accurate value of internodal conductivity for steady-state flow, assumes values between the integrated mean of the nodal conductivities and the conductivity of the upper node [26], depending on the form of relative conductivity function and internodal distance. Consequently, no simple averaging method can be accurate for a wide range of soil types and discretizations. In the presented examples the performance of simple methods varied significantly. For downward infiltration in dry soil or for upward flow upstream averaging overestimates the internodal conductivity. In our examples CC-UPS was more accurate than VC-UPS. The differences were particularly large in examples with multiple interfaces (C and E), where the accuracy of CC-UPS was often comparable to VC-SZYM and CC-SZYM. It seems that this differences come from the fact that in VC scheme the change in water content at highly permeable side of

the interface results in an immediate change in the part of the control volume located at the weakly permeable part of the interface, due to the assumption of the equilibrium of water potential across the interface. If the control volumes at the interface are large, considerable amounts of water can be transferred with unphysically high speed across the interface. In the CC-UPS scheme the interface coincides with the boundary between control volumes and harmonic averaging of the saturated conductivity (which gives more weight to the weakly permeable medium) partly compensates for the acceleration caused by upstream weighting of the relative conductivity.

The arithmetic mean often overestimates the internodal conductivity, although for very coarse discretizations it can actually underestimate it, leading to oscillations in the solution [25, 19]. In the examples presented here both VC-ARIT and CC-ARIT were more accurate than VC-UPS and showed good convergence properties in nearly all cases, i.e. the error clearly diminished with increasing number of nodes. However, the overprediction of infiltration and evaporation rates was significant, especially in Test Cases D and E on coarse grids. Here CC-ARIT clearly outperformed VC-ARIT, but in general the relative accuracy of those two schemes was highly problem-dependent. While accurate results can be obtained with arithmetic average using sufficiently refined grid near the boundaries and material interfaces [5], the use of averaging schemes based on Darcian mean can be advantageous, as it allows to obtain the same accuracy on coarser discretizations. This can be important especially when the solution domain contains a large number of interfaces and local refinement would lead to excessively large grid size. On the other hand, it is difficult to define a priori what grid size is fine enough to avoid significant errors in the solution.

The schemes based on geometric mean (VC-GEOM and CC-ROM) showed the largest variation in performance. They were very accurate in Test Case A for all discretizations and in Test Cases B and C for finer discretizations. However in the latter two cases their accuracy quickly deteriorated as the spatial step increased, sometimes leading to convergence problems. The resulting profiles of water content were far away from the reference solution. In the examples dealing with evaporation (D and E) both methods severely underestimated the evaporation rate. It can be shown that geometric mean is a good approximation of the integrated mean for fine-textured soils with parameter n in van Genuchten–Mualem function close to 1 [14]. On the other hand, the integrated mean is a good estimation of Darcian mean if the flow is dominated by capillary forces at the scale of a single gridblock, which

generally holds for small gridblock size [25]. As a result, the applicability of geometric mean is limited to relatively fine discretizations and finely textured soils. For coarse discretizations and/or coarse-textured soils the geometric mean severely underestimates the internodal conductivity, leading to unrealistic results and poor convergence. These shortcomings are also present in the scheme CC-ROM, although it is generally more accurate than VC-GEOM. Thus, geometric averaging cannot be considered as a robust approach.

All the presented schemes can be applied for 2D problems on rectangular grids, on condition that all porous materials within the solution domain are isotropic or orthotropic (characterized by diagonal conductivity tensor). The extension of cell-centered discretization to 2D is straightforward, while for vertex-centered approach additional consideration is necessary when computing flux between two nodes located along the material interface. In such a case one has to compute separately the fluxes at each side of the interface, using different material properties, and add them together in the balance equation. On the other hand, VC-SZYM scheme can be used to estimate the average conductivity between pairs of nodes arbitrarily oriented in space ($0 < \gamma < 1$), as long as the soil between them is homogeneous and isotropic. Thus it can be potentially applied in the framework of vertex centered finite volume schemes on unstructured grids. In control-volume finite element or box schemes, the water fluxes are computed for the faces of sub-control volumes using the average value of conductivity for the two nodes which are endpoints of the edge adjacent to the considered face. Integration of improved averaging schemes in such type of discretization will be the subject of future research by the authors.

Acknowledgements

The author A.S. would like to thank the German Research Foundation (DFG) for financial support of the project within the Cluster of Excellence in Simulation Technology (EXC 310/1) at the University of Stuttgart. Support from the International Research Training Group "Nonlinearities and Upscaling in Porous Media" (NUPUS) for the same author is kindly acknowledged here. Finally, the comments of four anonymous reviewers, which helped to improve the manuscript, are highly appreciated by the authors.

References

[1] R. Brooks, A. Corey, Hydraulic properties of porous media, Hydrology Paper 3, Colorado State University, Fort Collins, Colorado, USA, 1964.

[2] Y. Mualem, A new model for predicting the hydraulic conductivity of unsaturated porous media, Water Resources Research 12 (3) (1976) 513–522, doi:10.1029/WR012i003p00513.

[3] M. van Genuchten, A closed form equation for predicting the hydraulic conductivity of unsaturated soils, Soil Science Society of America Journal 44 (5) (1980) 892–898.

[4] M. Celia, E. Bouloutas, R. Zarba, A general mass-conservative numerical solution for the unsaturated flow equation, Water Resources Research 26 (7) (1990) 1483–1496.

[5] J. van Dam, R. Feddes, Numerical simulation of infiltration, evaporation and shallow groundwater levels with the Richards equation, Journal of Hydrology 233 (1) (2000) 72–85, doi:10.106/S0022-1694(00)00227-4.

[6] B. Brunone, M. Ferrante, N. Romano, A. Santini, Numerical simulations of one-dimensional infiltration into layered soils with the Richards' equation using different enstimates of the interlayer conductivity, Vadose Zone Journal 2 (2) (2003) 193–200, doi:10.2113/2.2.193.

[7] V. Lima-Vivancos, V. Voller, Two numerical methods for modeling variably saturated flow in layered media, Vadose Zone Journal 3 (2004) 1031–1037.

[8] J. Šimůnek, M. Šejna, H. Saito, M. Sakai, M. van Genuchten, The HYDRUS-1D software package for simulating the one-dimensional movement of water, heat and multiple solutes in variably-saturated media. Version 4.0, Department of Environmental Sciences, University of California Riverside, Riverside, California, 2008.

[9] B. Belfort, F. Lehmann, Comparison of equivalent conductivities for numerical simulation of one-dimensional unsaturated flow, Vadose Zone Journal 4 (4) (2005) 1191–1200, doi:10.2136/vzj2005.0007.

[10] H. Li, M. Farthing, C. Dawson, C. Miller, Local discontinuous Galerkin approximations to Richards equation, Advances in Water Resources 30 (3) (2007) 555–575.

[11] H. Li, M. Farthing, C. Miller, Adaptive local discontinuous Galerkin approximation to Richards equation, Advances in Water Resources 30 (9) (2007) 1883–1901.

[12] R. Haverkamp, M. Vauclin, A note on estimating finite difference interblock hydraulic conductivity values for transient unsaturated flow, Water Resources Research 15 (1) (1979) 181–187.

[13] R. Schnabel, E. Richie, Calculation of internodal conductances for unsaturated flow simulations, Soil Science Society of America Journal 48 (5) (1984) 1006–1010.

[14] J. Zaidel, D. Russo, Estimation of finite difference interblock conductivities for simulation of infiltration into initially dry soils, Water Resources Research 28 (9) (1992) 2285–2295, doi:10.1029/92WR00914.

[15] C. Miller, G. Williams, C. Kelley, M. Tocci, Robust solution of Richards equation for nonuniform porous media, Water Resources Research 34 (10) (1998) 2599–2610.

[16] D. Baker, M. Arnold, H. Scott, Some analytic and approximate Darcian means, Ground Water 37 (4) (1999) 532–538, doi:10.1111/j.1745-6584.1999.tb01139.x.

[17] R. Srivastava, A. Guzman-Guzman, Analysis of hydraulic conductivity averaging schemes for one-dimensional, steady-state unsaturated flow, Ground Water 33 (6) (1995) 946–952, doi:10.1111/j.1745-6584.

[18] J. Gastó, J. Grifoll, Y. Cohen, Estimation of internodal permeabilities for numerical simulations of unsaturated flows, Water Resources Research 38 (12) (2002) 1326, doi:10.1029/2002WR001529.

[19] A. Szymkiewicz, Approximation of internodal conductivities in numerical simulation of 1D infiltration, drainage and capillary rise in unsaturated soils, Water Resources Research 45 W10403, doi: 10.1029/2008WR007654.

[20] R. Mansell, L. Ma, L. Ahuja, S. Bloom, Adaptive grid refinement in numerical models for water flow and chemical transport in soil, Vadose Zone Journal 1 (2) (2002) 222–238.

[21] C. Miller, C. Abhishek, M. Farthing, A spatially and temporally adaptive solution of Richards' equation, Advances in Water Resources 29 (4) (2006) 525–545, doi:10.1016/j.advwatres.2005.06.008.

[22] G. Williams, C. Miller, C. Kelley, Transformation approaches for simulating flow in variably saturated porous media, Water Resources Research 36 (4) (2000) 923–934.

[23] P. Ross, Modeling soil water and solute transport – fast simplified numerical solutions, Agronomy Journal 95 (2003) 1352–1361.

[24] A. Warrick, Numerical approximation of Darcian flow through unsaturated soil, Water Resources Research 27 (1991) 1215–1222.

[25] D. Baker, Darcian weighted interblock conductivity means for vertical unsaturated flow, Ground Water 33 (1995) 385–390, doi:10.1111/j.1745-6584.1995.tb00294.x.

[26] D. Baker, A Darcian integral approximation to interblock hydraulic conductivity means in vertical infiltration, Computers and Geosciences 26 (5) (2000) 581–590, doi:10.1016/S0098-3004(99)00129-6.

[27] R. Hills, I. Porro, D. Hudson, P. Wierenga, Modeling one-dimensional infiltration into very dry soils: Model development and evaluation, Water Resources Research 25 (6) (1989) 1259–1269.

[28] N. Romano, B. Brunone, A. Santini, Numerical analysis of one-dimensional unsaturated flow in layered soils, Advances in Water Resources 21 (4) (1998) 315–324, doi:10.1016/S0309-1708(96)00059-0.

[29] P. Forsyth, Y. Wu, K. Pruess, Robust numerical methods for saturated unsaturated flow in heterogeneous media, Advances in Water Resources 18 (1) (1995) 25–38, doi:10.1016/0309-1708(95)00020-J.

[30] R. Helmig, R. Huber, Comparison of Galerkin-type discretization techniques for two-phase flow in heterogenous porous media, Advances in Water Resources 21 (8) (1998) 697–711.

Table 1: Parameters of soils used in numerical simulations

Soil	θ_R [−]	θ_S [−]	h_e or h_g [cm]	λ or n [−]	K_S [cm · s^{-1}]
BC-sand	0.020	0.417	7.25	0.592	$5.83 \cdot 10^{-3}$
BC-clay	0.056	0.423	34.25	0.127	$2.50 \cdot 10^{-5}$
VGM-sand	0.043	0.430	6.90	2.68	$8.25 \cdot 10^{-3}$
VGM-clay	0.007	0.360	200.0	1.09	$5.56 \cdot 10^{-6}$
Berino	0.0286	0.3658	35.7	2.239	$6.26 \cdot 10^{-3}$
Glendale	0.106	0.4686	96.2	1.3954	$1.52 \cdot 10^{-4}$
GAR-coarse	0.06	0.4	10.0	$\cdots$	$2.78 \cdot 10^{-3}$
GAR-fine	0.06	0.4	10.0	$\cdots$	$2.78 \cdot 10^{-4}$

Table 2: Errors of various averaging schemes for soils characterized by BCM functions – steady state problems

Scheme	$RMS(E_K)$ [−]	$\max(E_K)$ [−]	$\min(E_K)$ [−]	$RMS(E_{hc})$ [cm]
CC-ARIT	1.91	6.18	−0.24	–
CC-ROM	0.66	2.32	−2.77	18.15
CC-UPS	1.56	5.46	−2.55	–
CC-SZYM	0.08	1.34	−0.32	0.41

Table 3: Errors of various averaging schemes for soils characterized by VGM functions – steady state problems

Scheme	$RMS(E_K)$ [−]	$\max(E_K)$ [−]	$\min(E_K)$ [−]	$RMS(E_{hc})$ [cm]
CC-ARIT	3.21	10.37	−0.28	–
CC-ROM	1.78	5.58	−7.30	23.42
CC-UPS	1.94	7.88	−3.71	–
CC-SZYM	0.10	0.07	−0.51	1.31

Table 4: Error, number of time steps and computational time in simulations for Test Case A

Scheme	$\Delta z = 1$ cm				$\Delta z = 20$ cm				$\Delta z = 100$ cm			
	ERR_h) [cm]	ERR_θ [-]	$N_{\Delta t}$ [-]	Time [s]	ERR_h [cm]	ERR_θ [-]	$N_{\Delta t}$ [-]	Time [s]	ERR_h [cm]	ERR_θ [-]	$N_{\Delta t}$ [-]	Time [s]
CC-ARIT	1.19E–1	9.37E–4	1490	2.04	1.67E+0	6.33E–3	1418	1.20	6.00E+0	1.04E–2	1441	0.990
CC-ROM	1.21E–2	4.37E–5	1488	2.90	6.70E–1	3.17E–3	1477	1.30	1.24E+1	1.32E–2	1441	1.10
CC-UPS	2.18E–1	7.56E–4	1435	1.90	2.70E+0	1.22E–2	1489	1.22	1.04E+1	2.01E–2	1432	1.15
CC-SZYM	2.91E–2	9.19E–5	1488	2.18	9.10E–1	3.45E–3	1457	1.32	6.67E+0	2.19E–2	1432	1.20
VC-ARIT	1.16E–2	3.14E–5	1490	1.88	1.03E+0	5.78E-3	1477	1.14	2.72E+1	8.10E–2	1417	1.00
VC-GEOM	1.40E–2	3.76E–5	1488	2.96	7.58E–1	4.73E–3	1463	1.23	1.69E+1	7.17E–2	1511	1.08
VC-UPS	2.22E–1	7.83E–4	1433	1.86	2.39E+0	1.40E–2	1444	1.22	5.84E+0	6.62E–2	1459	1.09
VC-SZYM	2.98E–2	8.86E–5	1488	1.95	9.34E–1	6.26E–3	1482	1.25	5.45E+0	6.75E–2	1447	1.11
VC-BAKER	9.30E–3	2.44E–5	1488	2.01	9.39E–1	7.62E–3	1438	1.14	5.44E+0	6.75E–2	1447	1.11

Table 5: Error, number of time steps and computational time in simulations for Test Case B

Scheme	$\Delta z = 1$ cm				$\Delta z = 20$ cm				$\Delta z = 100$ cm			
	ERR_h [cm]	ERR_θ [-]	$N_{\Delta t}$ [-]	Time [s]	ERR_h [cm]	ERR_θ [-]	$N_{\Delta t}$ [-]	Time [s]	ERR_h [cm]	ERR_θ [-]	$N_{\Delta t}$ [-]	Time [s]
CC-ARIT	7.60E+2	6.58E–3	27339	108	3.79E+3	4.99E–2	2634	2.67	6.91E+3	8.15E–2	928	0.982
CC-ROM	2.46E+2	3.51E–3	25453	141	3.24E+3	1.58E–1	12019	38.5	3.21E+1	5.59E–2	1033	1.58
CC-UPS	9.04E+2	7.78E–3	23020	92.3	3.00E+3	2.72E–2	2599	2.71	5.80E+3	3.97E–2	966	0.983
CC-SZYM	5.55E+1	1.13E–3	28965	174	1.78E+3	8.85E–3	3017	6.69	4.67E+3	4.18E–2	981	1.96
VC-ARIT	7.88E+2	5.81E–3	27521	112	2.63E+3	4.02E–2	2914	2.93	4.63E+1	9.29E–2	1116	1.06
VC-GEOM	7.73E+1	1.85E–3	23272	116	4.09E+3	1.20E–1	13710	21.9	did not converge			
VC-UPS	1.16E+3	1.29E–2	22986	92.7	3.03E+3	5.30E–2	2765	2.81	5.79E+1	1.01E–1	1027	1.01
VC-SZYM	2.69E+2	8.95E–4	28969	148	9.88E+1	2.05E–2	3534	3.89	2.00E+1	5.50E–2	1284	1.37
VC-BAKER	2.70E+2	8.71E–4	28966	153	8.81E+1	2.02E–2	3403	3.91	1.96E+1	5.41E–2	1366	1.31
VC-GASTO	2.56E+2	8.49E–4	29017	179	not applicable				not applicable			

Table 6: Error, number of time steps and computational time in simulations for Test Case C

Scheme	$\Delta z = 1$ cm			$\Delta z = 10$ cm			$\Delta z = 20$ cm		
	REL_{INF} [%]	$N_{\Delta t}$ [-]	Time [s]	REL_{INF} [%]	$N_{\Delta t}$ [-]	Time [s]	REL_{INF} [%]	$N_{\Delta t}$ [-]	Time [s]
CC-ARIT	4.75	3004	3.82	30.4	749	0.902	42.7	651	0.640
CC-ROM	0.142	4376	10.3	−67.3	540	0.671	−67.7	547	0.671
CC-UPS	4.75	2728	3.58	9.99	736	0.748	5.60	606	0.499
CC-SZYM	1.91	1812	4.19	0.142	689	1.34	−1.77	616	0.998
VC-ARIT	3.19	2967	4.55	13.5	730	1.31	20.9	595	0.515
VC-GEOM	0.709	3265	6.72	−75.7	530	0.640	−85.3	530	0.468
VC-UPS	5.95	2796	3.57	24.7	758	0.751	17.6	617	0.702
VC-SZYM	1.91	1766	2.89	−0.425	595	0.640	−3.69	535	0.515
VC-GASTO	2.48	4834	12.8	2.48	849	1.73	4.96	637	0.624

Table 7: Error, number of time steps and computational time in simulations for Test Case D

Scheme	$\Delta z = 1$ cm			$\Delta z = 5$ cm			$\Delta z = 25$ cm		
	REL_{EV} [%]	$N_{\Delta t}$ [-]	Time [s]	REL_{EV} [%]	$N_{\Delta t}$ [-]	Time [s]	REL_{EV} [%]	$N_{\Delta t}$ [-]	Time [s]
CC-ARIT	21.98	555	0.89	114.30	542	0.530	733	539	0.404
CC-ROM	−85.23	536	0.81	−96.35	537	0.593	−98.4	537	0.381
CC-UPS	46.22	564	0.64	207.95	544	0.478	2320	542	0.347
CC-SZYM	1.81	553	0.80	−7.19	538	0.756	−18.4	537	0.488
VC-ARIT	25.92	555	0.97	150	541	0.655	8200	540	0.358
VC-GEOM	−91.87	537	0.54	−97.9	537	0.414	−99.7	537	0.337
VC-UPS	51.36	563	0.65	268	544	0.546	16200	540	0.318
VC-SZYM	0.10	548	0.78	−6.98	538	0.702	−39.0	537	0.484
VC-GASTO	−30.80	537	0.89	−61.9	534	0.812	not applicable		

Table 8: Error, number of time steps and computational time in simulations for Test Case E

Scheme	$\Delta z = 1$ cm			$\Delta z = 10$ cm			$\Delta z = 40$ cm		
	REL_{EV} [%]	$N_{\Delta t}$ [s]	Time [%]	REL_{EV} [s]	$N_{\Delta t}$ [%]	Time [s]	REL_{EV}	$N_{\Delta t}$	Time
CC-ARIT	19.7	631	0.827	400	274	0.255	2220	171	0.125
CC-ROM	−58.9	687	1.55	−59.1	331	0.403	−59.1	223	0.234
CC-UPS	2.11	673	0.952	−9.63	306	0.579	14.3	211	0.187
CC-SZYM	3.09	1020	2.51	−2.33	280	0.404	−9.60	208	0.249
VC-ARIT	16.4	623	0.952	237	265	0.436	15300	156	0.125
VC-GEOM	−59.3	636	1.39	−63.9	313	0.343	−78.2	188	0.187
VC-UPS	29.1	673	1.25	469	262	0.269	30500	155	0.171
VC-SZYM	3.07	1011	2.14	−5.25	263	0.296	−37.6	175	0.156
VC-GASTO	−43.0	682	1.88	not applicable			not applicable		

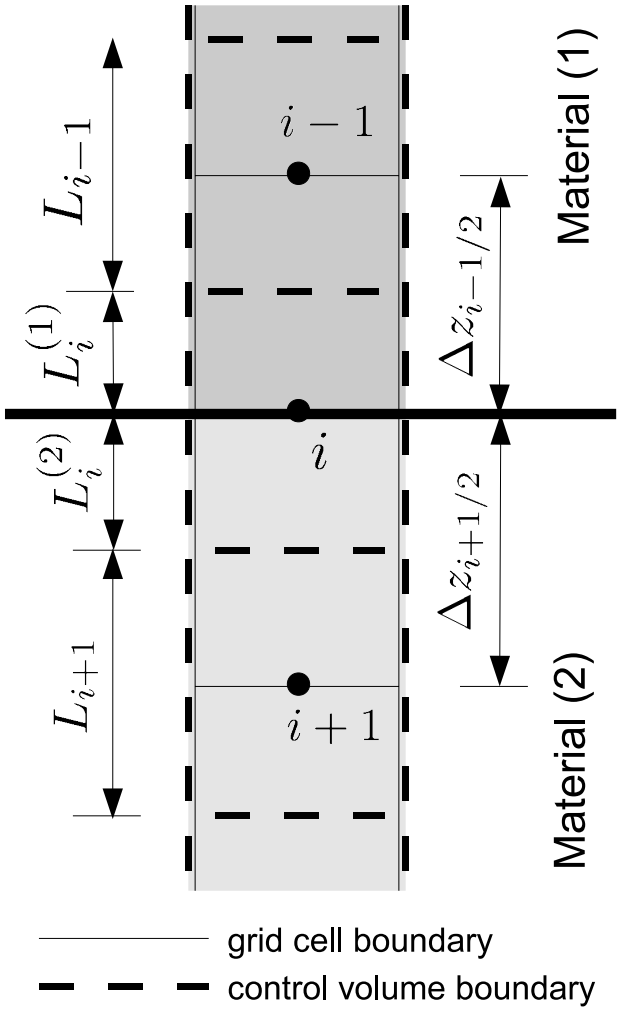

Figure 1: Vertex-centered spatial discretization.

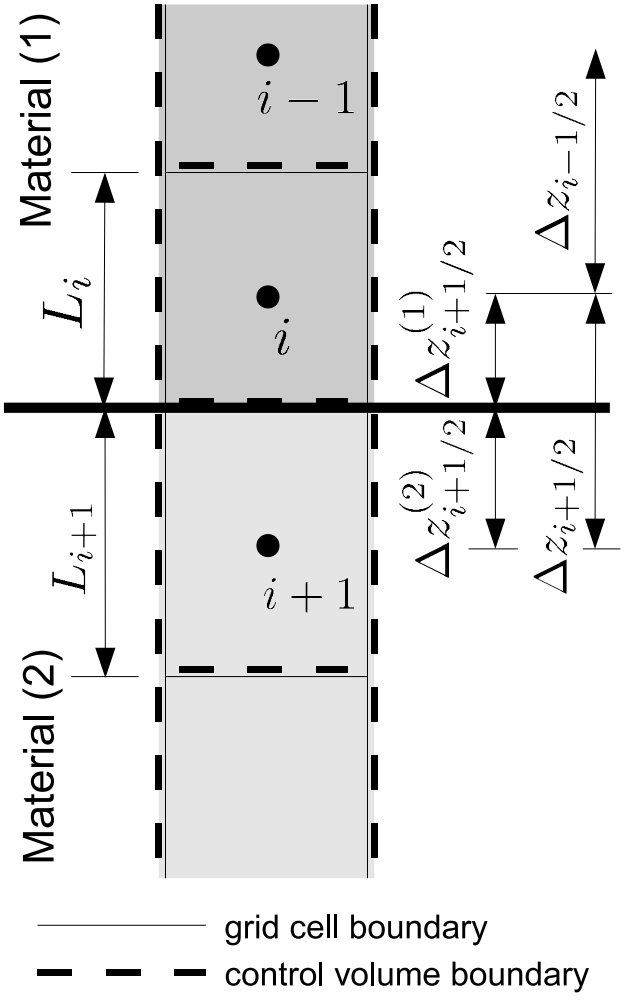

Figure 2: Cell-centered spatial discretization.

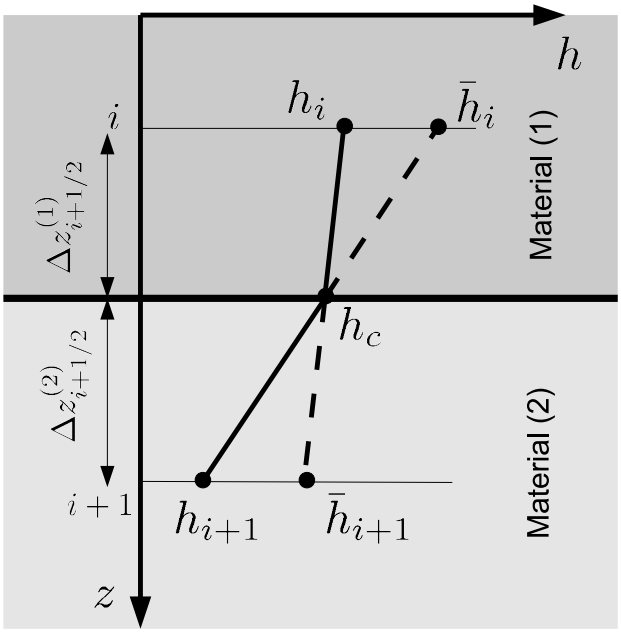

Figure 3: Spatial discretization at the material interface in the cell-centered approaches CC-ROM and CC-SZYM.

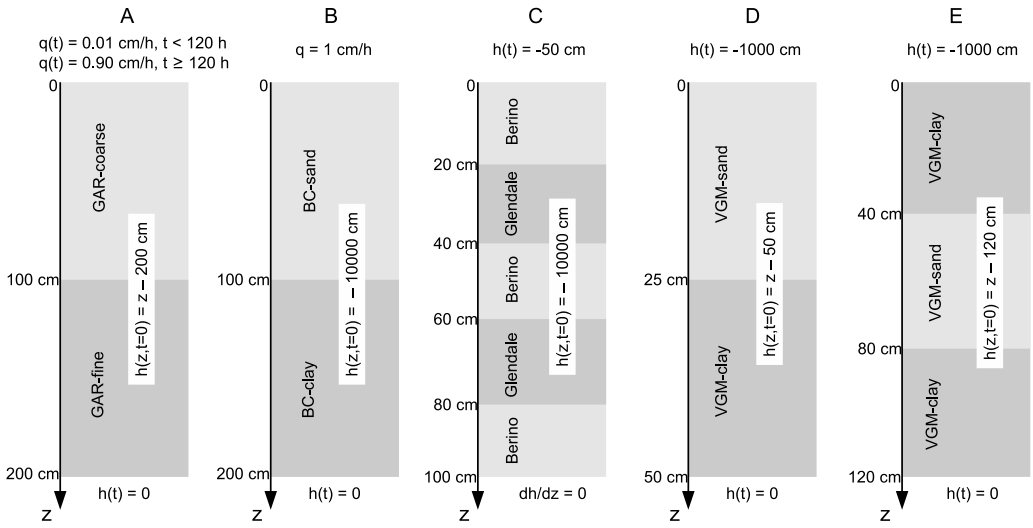

Figure 4: Geometry and initial-boundary conditions used in numerical examples.

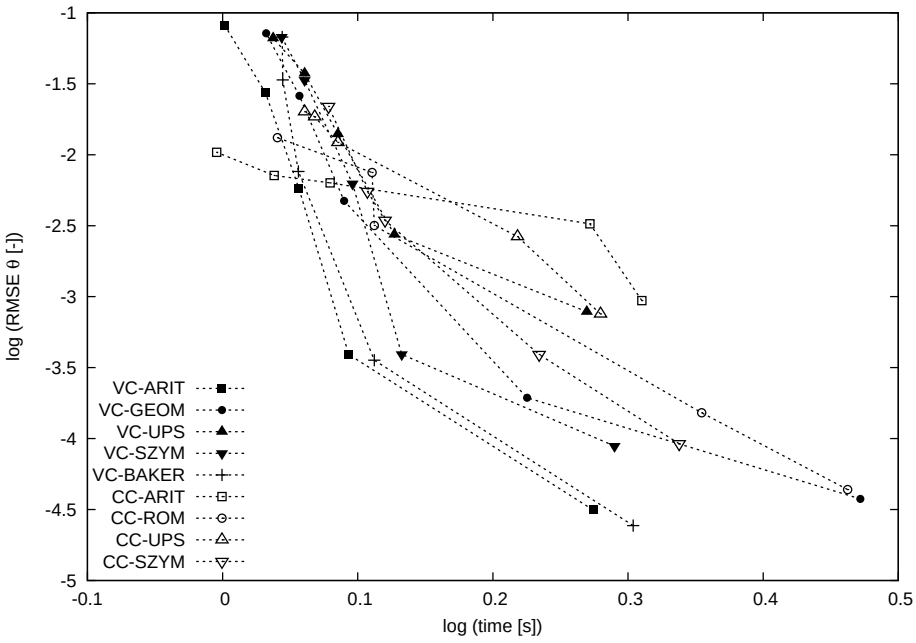

Figure 5: Test Case A: error vs. computational time for various schemes.

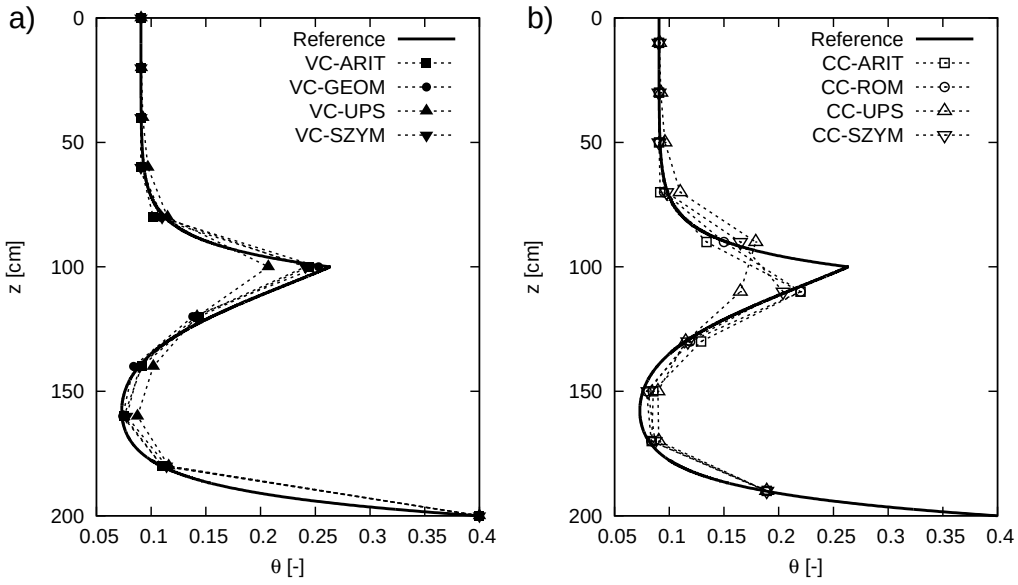

Figure 6: Test Case A: water content profiles obtained with VC (a) and CC (b) schemes ($t = 130$ h, $\Delta z = 20$ cm).

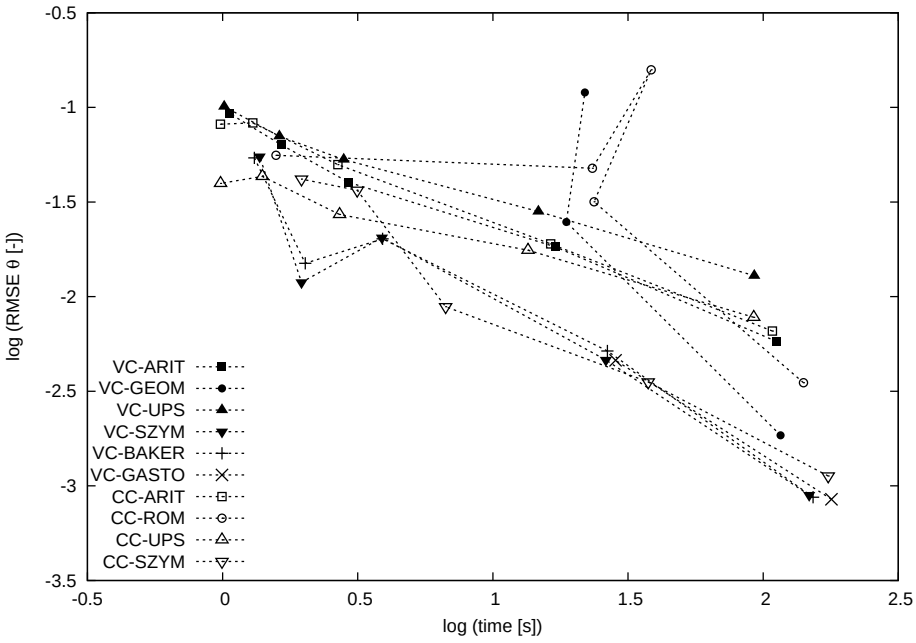

Figure 7: Test Case B: error vs. computational time for various schemes.

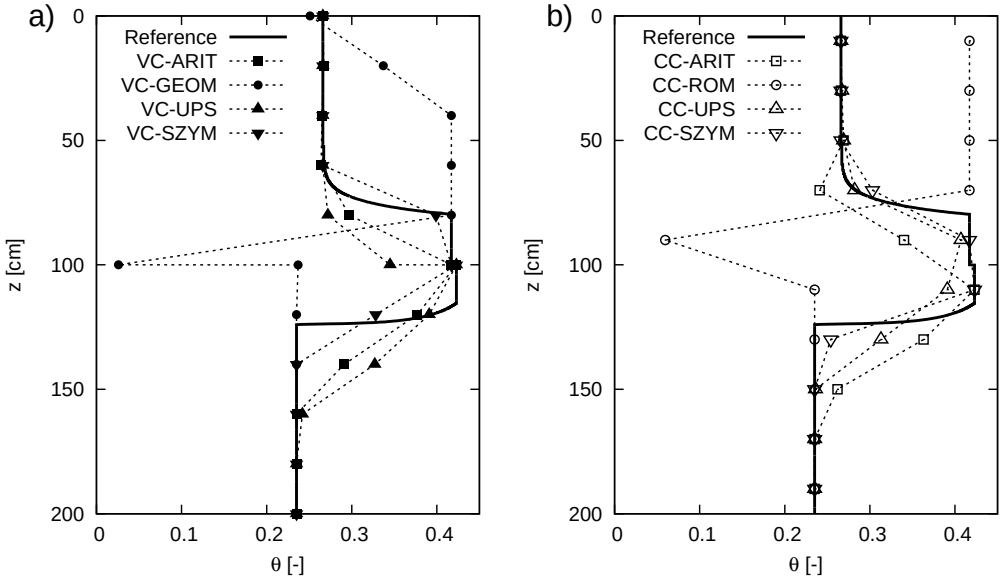

Figure 8: Test Case B: water content profiles obtained with VC (a) and CC (b) schemes ($t = 32$ h, $\Delta z = 20$ cm).

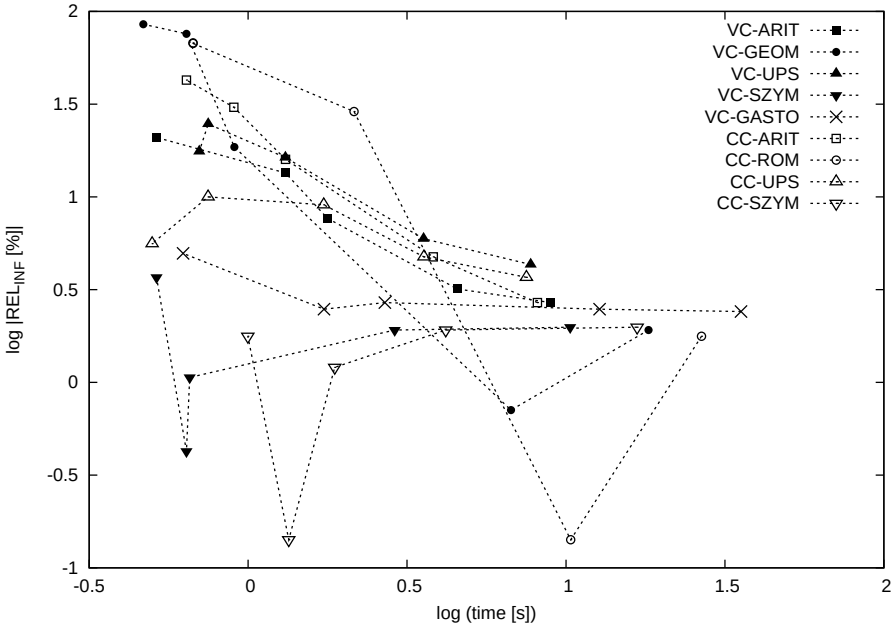

Figure 9: Test Case C: error (REL_{INF}) vs. computational time for various schemes.

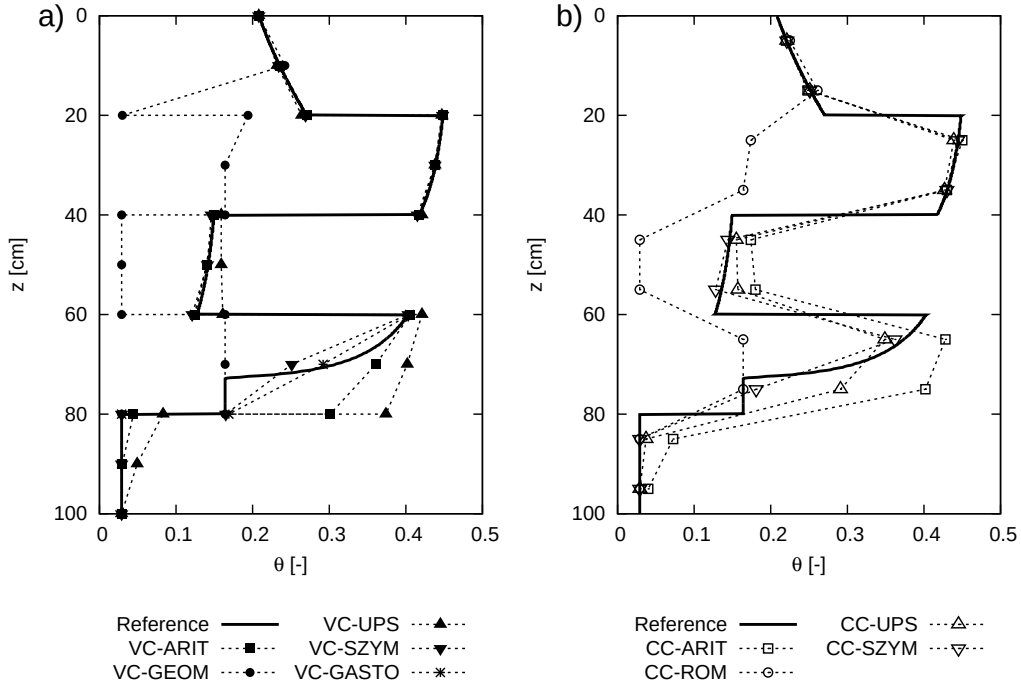

Figure 10: Test Case C: water content profiles obtained with VC (a) and CC (b) schemes ($t = 48$ h, $\Delta z = 10$ cm).

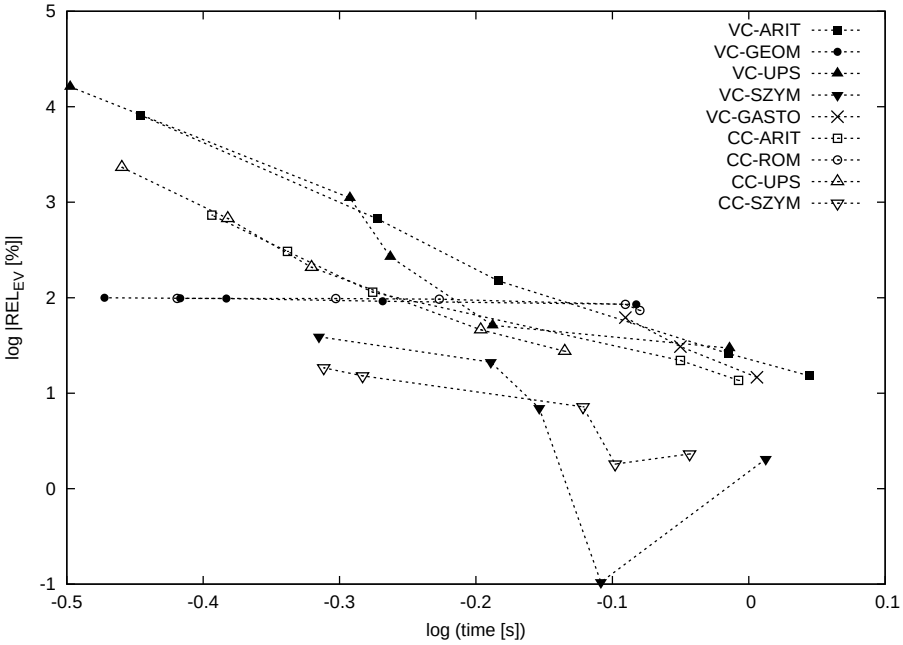

Figure 11: Test Case D: error (REL_{EV}) vs. computational time for various schemes.

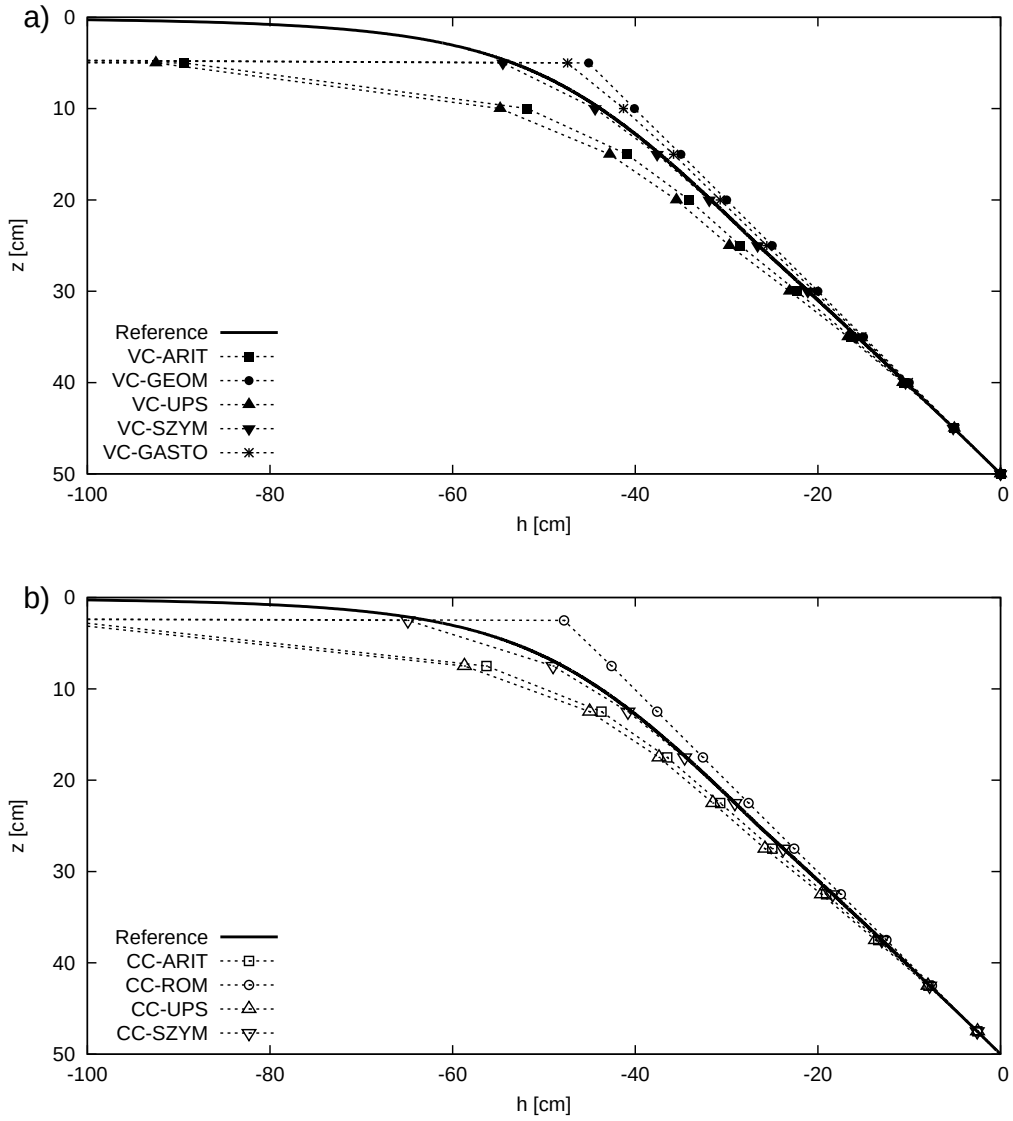

Figure 12: Test Case D: water potential head profiles obtained with VC (a) and CC (b) schemes ($t = 240$ h, $\Delta z = 5$ cm).

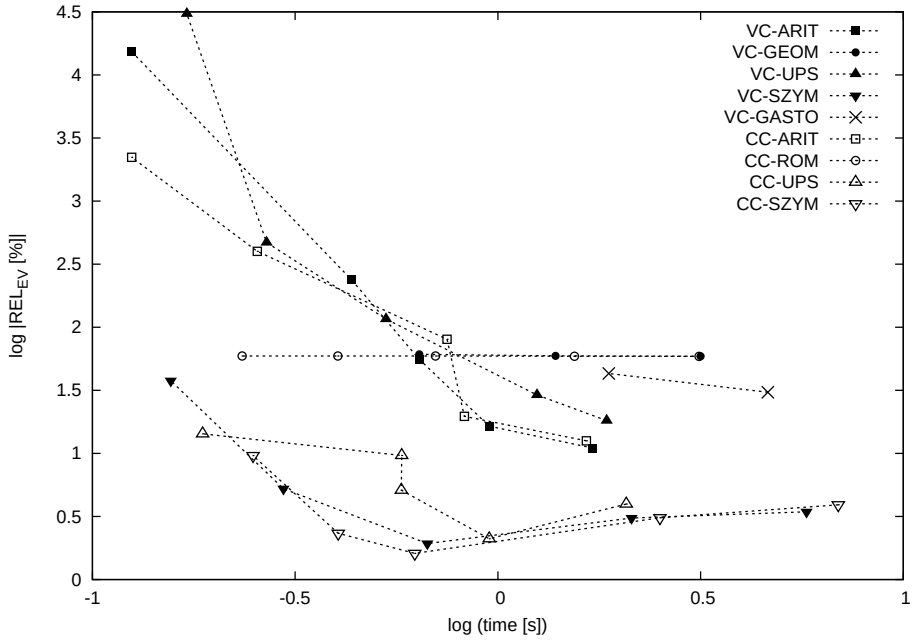

Figure 13: Test Case E: error (REL_{EV}) vs. computational time for various schemes.

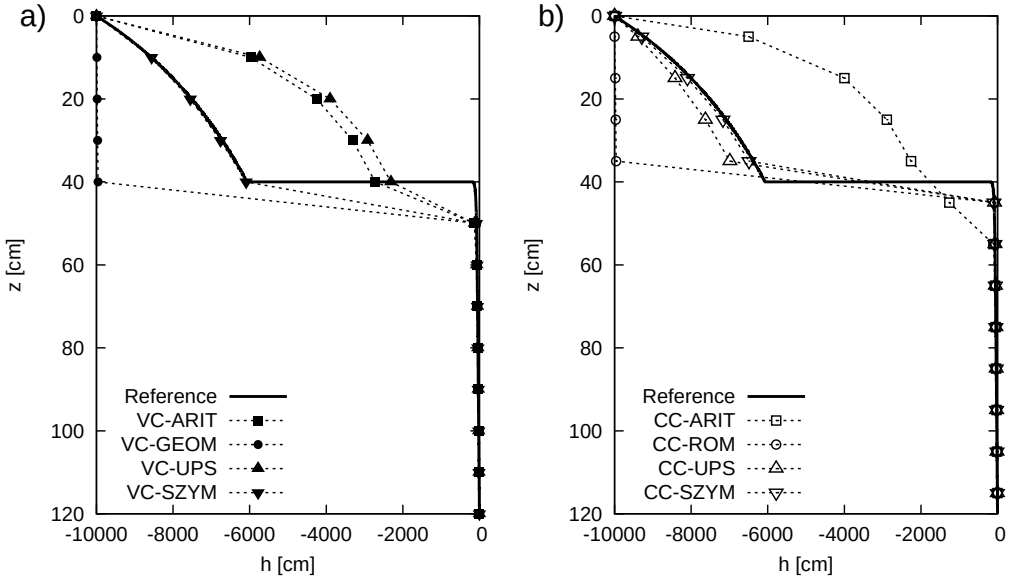

Figure 14: Test Case E: water potential head profiles obtained with VC (a) and CC (b) schemes ($t = 50000$ h, $\Delta z = 10$ cm).